Optics
2013; 2(5): 51-60
Published online September 20, 2013 (http://www.sciencepublishinggroup.com/j/optics)
doi: 10.11648/j.optics.20130205.11

Fourier-Bessel analysis of polar space symmetric photonic crystal; resonator modes and heterostructure

Scott Ronald. Newman, Robert Claude. Gauthier*

Dept. of Electronics, Carleton University, Ottawa, Ontario Canada K1S 5B6

Email address:
snewman@doe.carleton.ca (S. R. Newman), gauthier@doe.carleton.ca (R. C. Gauthier)

To cite this article:
Scott Ronald. Newman, Robert Claude. Gauthier. Fourier-Bessel Analysis of Polar Space Symmetric Photonic Crystal; Resonator Modes and Heterostructure. *Optics.* Vol. 2, No. 5, 2013, pp. 51-60. doi: 10.11648/j.optics.20130205.11

Abstract: A Fourier-Bessel equivalent of the plane wave technique is employed to theoretically analyze a circular photonic crystal structure containing both radial and rotational periodicity. The presence of the 12-fold rotational symmetry in the dielectric profile results in a 12-times reduction in the order of the matrix diagonalized when cast using the Fourier-Bessel basis functions. In addition, the Fourier-Bessel technique is highly suited for extracting the localized modes as it can be tuned to solve for a particular mode order. The possibility of using the circular structure as the defect region of a hexagonal array is also examined by studying the localized states obtained in a heterostructure configuration.

Keywords: Photonic Quasi-Crystal, Fourier-Bessel, Steady States, Heterostructure, Circular Symmetric Mode Solver, Eigenvalue Method

1. Introduction

Photonic crystals are generally regarded as translationally symmetric high dielectric contrast optical structures configured in one, two or three dimensions. Due to the translational symmetry, the rotational symmetry of the dielectric is limited to a maximum order of 6. Because of the low rotational order, wide variations in the band gap versus direction are often encountered and one must carefully design the dielectric layout, dielectric contrast and select the optical polarization in order to achieve large band gaps[1]. It has been recognized that higher order rotational symmetry photonic crystal structures are available, that the higher rotational symmetry provides a more uniform transmission spectrum versus propagation angle (for waves passing at normal incidence through the center of the dielectric pattern) and that localized states are naturally present[2]. Structures of this nature have come to be known as aperiodic crystals and quasi-crystals. The most common photonic quasi-crystal patterns have 8, 10, or 12 fold rotational symmetry and are designed with uniform circular inclusions.

Circular photonic crystals have been analyzed in a number of configurations demonstrating that structures with uniform circular holes (or rods) arranged in rings can show form birefringence[3], an array of centrally localized states [3, 4], and isotropic gaps in the transmission spectrum[5]. Massaroet. al. [6], have shown that these structures can be used to enhance the second harmonic generation through the use of available whispering gallery modes. These structures typically maintain uniform hole spacing in both angular and radial directions and the rotational symmetry dictated by the number of holes on the first ring. Several researchers have considered introducing optical waveguides into these structures for excitation and recovery of light coupled with a mode type[7]. Lasing properties are a common application examined in addition to standard resonator designs used in filtering [8, 9].

Over the years several reported circular photonic crystal structures have contained features that vary in size in relation to their distance from the center. Zarbakhashet. al. [10], considered a rod pattern with larger rods towards the center and a hole pattern with larger holes towards the exterior. The overall structure, although curved retained a hexagonal arrangement of the features. They showed the presence of gaps in the transmission spectrum and how a semi-circular segment could be used as a lens to focus an incident beam to the diffraction limit. Chaloupkaet. al. [11], explored the effects of keeping the number of holes constant within the radial rings. However, the increasing angular hole width was not related to the radial distance, and periodicity in the radial direction was not retained. The work showed that masking out the central region provided access to a large number of higher order modes in addition

to the traditional monopole, dipole and quadrupoles associated with the central states. The structure may also readily support high order whispering gallery modes and find applications in microcavity laser designs[12].

The structures examined in this work contain periodicity in both angular and radial directions where the angular symmetry order does not change with increasing radius. As a result of the imposed symmetry the angular arc length and radial extent of the holes are constant when using the center of the structure as the polar coordinate origin. The structures are created using simple generating functions when compared to other techniques such as matching rules[13], projections[14] and substitution[15] for generating higher order rotationally symmetric quasi-crystal patterns. These structures have been encountered in a number of published papers [16, 17, 18, 19] and the cavity properties examined through finite-difference time-domain (FDTD) simulations. In this paper we examine the localized state space of a hole structure in silicon that has periodicity of 12 in both the angular and radial directions. We further proceed to demonstrate that the structures are compatible with translationally symmetry photonic crystals in heterostructure arrangements with the quasi-crystal as the defect region of a hexagonal array. The analysis is performed using a newly developed Fourier-Bessel polar coordinate equivalent of the plane wave technique that was motivated by the presence of the rotational symmetry in photonic crystals[20].

2. Dielectric Profile

The dielectric profiles of interest in this paper are structures that contain periodicity in both the radial and angular directions of a polar coordinate system. The background dielectric is silicon with a relative dielectric constant, $\epsilon_{r,Si} = 12.1104$, and the features, holes, are air with $\epsilon_{r,o} = 1.000$. The structures produced can be considered as circular photonic crystals due to the rotational symmetry. The structures, when extended radially, are aperiodic due to the presence of long range order while lacking translational symmetry. There are many mathematical expressions which can be used to generate dual periodic structures. The expression used in this work is given in (1) where the center of the polar coordinate system corresponds to the center of the dielectric profile:

$$\epsilon_{r,o}(r,\varphi) \Leftrightarrow \epsilon_{r,o}\, cos(\pi\vartheta_r r) cos\left(\frac{\vartheta_\varphi}{2}\varphi\right)\Big]_A^B \qquad (1)$$

The angular rotation order is determined through the integer ϑ_φ and the radial periodicity is determined from the radial spatial frequency $\vartheta_r = {}^{N_r}/_{R}$ where N_r is an integer and R is the radial extent of the circularly symmetric structure. In (1), the product of the cosine functions determines the low dielectric regions when the values fall within the range limit (A, B). The circular photonic crystal pattern that is the focus of this work, Fig. 1 (Left), was produced with $(N_r, \vartheta_\varphi) = (12, 12)$, and $(A, B) = (-0.5, 0.5)$; discretization of the structure was done over a 3.91 μm radius disk. The radius of 3.91 μm was chosen to

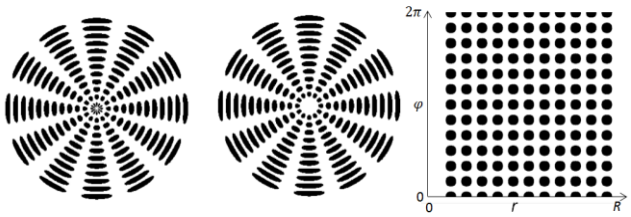

Figure 1. *(Left) Circular photonic crystal with* $(N_r, \vartheta_\varphi) = (12, 12)$, $(A, B) = (-0.5, 0.5)$ *defined over a radius of 3.91 μm and discretized on a 200 points per micron grid. (Center) Dielectric profile with the first ring of holes replaced with silicon. (Right) Circularly symmetric dielectric profile plotted with r along the abscissa axis and φ along the ordinate axis. The structures show periodicity along the two orthogonal axes and near circular holes produced in a mapped representation.*

scale the strongest monopole, shown later, to a wavelength of 1.55 μm. The black and white regions in Fig. 1 correspond to the air and background silicon respectively. In order to remove the fine features located in the center of the structure the central region is masked out, a design feature commonly encountered in circular photonic crystal structures[9]. Fig. 1 (Center) shows the dielectric profile when the first ring of holes is removed; all other properties of the dielectric structure are retained. Fig. 1 (Right), shows the dielectric profile with the radial dependence plotted along the abscissa axis and the angular dependence plotted along the ordinate axis. In this representation, the air holes are nearly circular in shape and the structure maps to a square array. This representation increases the viewing resolution in the central region. Both presentations of Fig. 1 are useful in the development and discussion. In the analysis leading to this presentation we have considered many different combinations of the generating parameters in (1) as well as an alternate expression which produces "square" holes in a circular array. The results presented here are representative of the general findings for these structures and the modeling technique. For any one particular application, structure parameters $(N_r, \vartheta_\varphi, A, B)$ would need to be selected as well as the scale factor in order to obtain the modal properties at the desired wavelength. Since the structures examined here contain holes in a high dielectric background and restricted to the 2-D (x, y) plane the TE polarization with H_z parallel to z-axis is chosen. The analysis technique can be easily extended for the TM polarization and for structures composed of high dielectric rods.

3. Theoretical Development

It is well established that when a photonic crystal contains translational symmetry the plane-wave expansion technique can be applied to Maxwell's wave equation to obtain information on the available states and field distributions[21].

When the structure contains an intentional defect the band structure can provide information on the states localized to the defect. These calculations are done using a periodically repeated super cell where the defect is surrounded by several periods of the unaltered array. The super cell required is large enough to ensure negligible fields at the cell boundary for the localized states. It has recently been shown that for circularly symmetric photonic crystals, a Fourier-Bessel (FB) equivalent of the plane-wave expansion method will directly provide the defect state information in the structure and does not require the periodic repetition of the unit super cell[22]. In addition the FB technique can be tuned to search for a specific mode type (monopole, dipole, quadrupole, …) making this technique ideally suited for the modal analysis of the structures displayed in Fig. 1. In the case of the TE polarization the governing equation for the H_z field component is[22]:

$$\frac{1}{r}\left(\frac{\partial}{\partial r}\left[\frac{r}{\epsilon}\left(-\frac{\partial H_z}{\partial r}\right)\right]-\frac{\partial}{\partial \varphi}\left[\frac{1}{r\epsilon}\frac{\partial H_z}{\partial \varphi}\right]\right)=\left(\frac{\omega}{c}\right)^2 H_z \qquad (2)$$

The inverse of the dielectric profile, $\frac{1}{\varepsilon}$, is expanded in a Fourier-Bessel series in which the r dependence is expressed using the lowest order Bessel functions, $J_o\left(\rho_n \frac{r}{R}\right)$, where ρ_n is the n[th] zero crossing of the Bessel function and R, the radius of the dielectric profile, serves as a scaling factor such that $0 \le \left[\frac{r}{R}=r'\right] \le 1$ conserves the orthogonality of the Bessel functions over the integration interval of the dielectric profile. This also highlights the fact that the traditional scaling rules for photonic crystal analysis using the plane-wave technique also apply to the FB technique. The angular coordinate dependence is expanded in exponentials of the form $e^{-jm\varphi}$ where m is any integer, $m=\{0,\pm1,\pm2,\pm3,\dots\}$. The expression for the inverse dielectric expansion makes use of two indices, (m,n) with expansion coefficients, $\kappa^{\epsilon}_{m,n}$:

$$\frac{1}{\epsilon}=\sum_{m,n}\kappa^{\epsilon}_{m,n}J_o\left(\frac{\rho_n r}{R}\right)e^{-jm\varphi} \qquad (3)$$

The H_z field component is also expanded using the Fourier-Bessel basis functions using the (p,q) indices and the expansion coefficients, $\kappa^{H}_{p,q}$:

$$H_z=\sum_{p,q}\kappa^{H}_{p,q}J_o\left(\frac{\rho_q r}{R}\right)e^{-jp\varphi} \qquad (4)$$

It should be noted that the field expression (4) does not contain a propagating factor with wavevector$\vec{k}$ introduced in a complex exponential. This emphasizes the fact that the FB technique applied here is used to determine only the steady (standing wave) states of the structure that are not propagated in the 2-D polar plane. We refer to this as the Gamma point FB calculation. The introduction of the expansions, (3) and (4), in the field component expression (2) and taking appropriate derivatives gives the following:

$$\sum_{m,n,p,q}\kappa^{H}_{p,q}\kappa^{\epsilon}_{m,n}\left[\frac{\left(\frac{r^2\rho_q^2}{R^2}+p^2+mp\right)}{r^2}J_o\left(\frac{\rho_q r}{R}\right)J_o\left(\frac{\rho_n r}{R}\right)-\frac{\rho_q\rho_n}{R^2}J_1\left(\frac{\rho_q r}{R}\right)J_1\left(\frac{\rho_n r}{R}\right)\right]e^{-j(p+m)\varphi}=\left(\frac{\omega}{c}\right)^2\sum_{p,q}\kappa^{H}_{p,q}J_o\left(\frac{\rho_q r}{R}\right)e^{-jp\varphi} \qquad (5)$$

The right hand side of (5) contains a summation over the field attributes and as such the exponential contains only the field's angular index p. The exponential on the left side shows a mixing of the rotational orders of both the field and inverse dielectric in the combined index $(p+m)$. In addition the expansion coefficients of the inverse dielectric and field are multiplied together. These two properties play a key role in simplifying the FB analysis technique as the next step is to make use of the orthogonality of the basis functions and recast equation (5) into the eigenvalue expression, (6). The orthogonality integration is performed over a disc of radius R and the eigenvalues, the normalized frequencies$\left(\frac{\omega R}{2\pi c}\right)$, for the steady states are obtained[22]:

$$\sum_{m,n,p,q}\kappa^{\varepsilon}_{p'-m,n}\left(\rho_n^2 S_{q,q',n}+mpT_{q,q',n}-\rho_n\rho_q U_{q,q',n}\right)\kappa^{H}_{p,q}=\left(\frac{\omega R}{2\pi c}\right)^2\kappa^{H}_{p',q'} \qquad (6)$$

Where $\left(S_{q,q',n},T_{q,q',n},U_{q,q',n}\right)$ are defined by the following integrals:

$$S_{q,q',n}=\frac{8\pi^2\int_0^1 r' J_o(\rho_q r')J_o\left(\rho_{q'}r'\right)J_o(\rho_n r')dr'}{\left[J_1\left(\rho_{q'}\right)\right]^2}$$
$$T_{q,q',n}=\frac{8\pi^2\int_0^1\left(\frac{1}{r'}\right)J_o(\rho_q r')J_o\left(\rho_{q'}r'\right)J_o(\rho_n r')dr'}{\left[J_1\left(\rho_{q'}\right)\right]^2} \qquad (7)$$
$$U_{q,q',n}=\frac{8\pi^2\int_0^1 r' J_o(\rho_q r')J_1\left(\rho_{q'}r'\right)J_1(\rho_n r')dr'}{\left[J_1\left(\rho_{q'}\right)\right]^2}$$

The integrals in (7) are independent of the dielectric profile and field distribution, allowing them to be evaluated and stored for use in the analysis of any circularly symmetric photonic crystal structure. The FB technique can also be applied directly to translationally symmetric photonic crystals in order to determine the steady states localized to an intentionally introduced defect. Within the translational domain a circular super cell with the defect region at the center is chosen. The super cell is large enough to ensure negligible fields of the steady sates.

It is also worth noting that the traditional FB decomposition in polar space links the order of the Bessel function to the order of the exponential with basis functions of the form$J_m\left(\frac{\rho_m r}{R}\right)e^{-jm\varphi}$. When these particular basis functions are used and after introduced into Maxwell's wave equation, the radial derivatives will produce Bessel orders of $m, m+1, m+2, \dots$ for all values ofm or p. The number of integrals forming the (STU) tables would need to be increased to accommodate all Bessel orders. An alternate approach to drastically increasing the (STU) space

is to apply the Bessel recursion relationships and reduce all Bessel orders to either 0 or 1. Directly using the basis functions and expansions in (2) and (3) simplifies the mathematical process.

The inverse dielectric for the structure in Fig. 1 (Center) was expanded using 250 zero crossing orders of the Bessel and 361 angular components, $(n, m) \Longrightarrow (1 \rightarrow 250, -180 \rightarrow 180)$. Tests (not presented) indicate sufficient converge of the computations using the orders indicated for the structures examined. This generates 90,250 expansion coefficients. Information on the nature

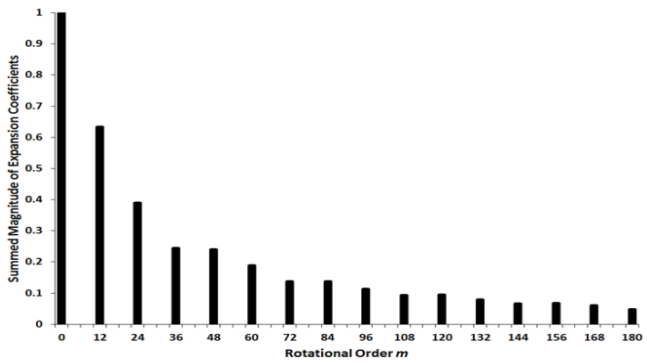

Figure 2. *Summed magnitude of the Fourier-Bessel decomposition coefficients for the dielectric under study plotted versus rotational order m (positive side only). The circular dielectric is 12-fold and thus the only non-zero expansion coefficients occur when m is an integer multiple of ±12.*

of the expansion coefficients can be obtained by examining them based on the rotational order they are associated with.Due to the large number of expansion coefficients involved, Fig. 2 is plotted with the rotational order index m along the abscissa axis for positive values of m and the summed magnitude of the expansion coefficients, $\left| \kappa^{\epsilon}_{m,n} \right|$ for each rotational order along the ordinate axis. Due to the rotational symmetry of the dielectric, the negative m expansion coefficients are the complex conjugate of the coefficients with the positive m indices. The dielectric profile has a 12-fold rotational symmetry, $\vartheta_{\varphi} = 12$ and as a result the only possible non-zero expansion coefficients are those for $m = (0, \pm 12, \pm 24, \pm 36, \ldots)$. The presence of a large number of zero values for the dielectric expansion introduces a large number of zero elements in the eigenvalue equation since the expansion coefficients of the field are multiplied by the expansion coefficients of the inverse dielectric, equations (5) and (6). This means that the rotation order index of the inverse dielectric coefficient in (6),$(p' - m)$, must be equal to a symmetry order of the dielectric, here $(0, \pm 12, \pm 24, \pm 36, \ldots)$ in order to be non-zero. The combined presence of the large number of zero elements in the matrix and the restriction on the index $(p' - m)$ imposed by the circular symmetry of the dielectric allows the eigenvalue matrix to be segmented into smaller units, where each unit represents a particular mode type (monopole, dipole, quadrupole, …). As a result of the 12-fold circular dielectric symmetry and the imposed circular symmetry of the mode orders, the order of the eigenvalue matrix for the monopoles is reduced by a factor of 12. Higher order modes have the matrix order reduced by a factor of 6. However, the matrix for higher order modes can be further segmented into two matrices of half the order and solved independently of each other. Therefore, the determination of the steady states of the circular dielectric structure using the FB technique can be very efficient even when large dielectric profiles are examined with several thousand expansion terms as the process can be tuned for a particular mode type.

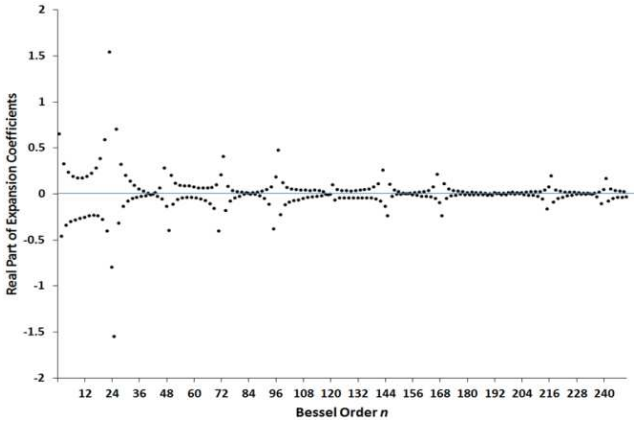

Figure 3. *Real part of the Fourier-Bessel expansion coefficients for the dielectric of Fig. 1 (Center) plotted as a function of the zero crossing order, n, for the rotational order $m = 0$. Due to the half cycle nature of the Bessel zero crossing indexing and the radial periodicity of 12 for the dielectric, the expansion coefficients reach extremes in the vicinity of 24, 48, 72, ….. Missing extremums are also observed and result from the interplay of the dielectric symmetry and low dielectric hole shape.*

Fig. 3 shows the real part of the expansion coefficients for the inverse dielectric plotted along the ordinate axis versus the zero crossing order n of the Bessel function for $m = 0$. The dielectric structure, with the exception of the removal of the inner most ring of holes, has a radial periodicity of 12. Since the Bessel function orders relate to half cycles for the zero crossings, the expansion coefficients reach extremes (+ and -) in the regions of $n = 24, 48, 72, \ldots$ which correspond to $12, 24, 36, \ldots$ full cycles. The alternating sign of the real part of the expansion coefficients ensures that the higher order contributions nearly cancel to restore the center dielectric value when used in (3). On occasion there are missing orders in the expansion coefficients of n for given orders of m that result from the interplay that exists between the radial symmetry of the dielectric structure and the shape of the low dielectric regions. For instance the Bessel expansions show missing orders in the vicinity of n = 192 for the rotational order m = 0.

4. Steady States

In order to determine the steady states for the dielectric under study, the inverse dielectric expansion coefficients are introduced along with the unknown expansion coefficients of the field into (6). The eigenmatrix is then solved for the monopole, dipole and quadrupole mode groups. The huge

complex matrices are easily handled on a desk top PC with 8 Gigs of memory running MATLAB©. The number of states returned for each mode type is related to the order of the matrix that is diagonalized. For monopole computations the matrix has order 7781 and thus 7781 eigenvalues are obtained. From these 69 correspond to wavelengths inthe 1.0 μm ≤ λ ≤ 2.5 μm range (normalized frequency range of 3.91 to 1.564). These particular modes can have field expansion coefficients that are non-zero for rotational orders $p = (0, \pm 12, \pm 24, \pm 36, \ldots)$. Within these modes, some will show a very strong monopole behavior as the expansion coefficients with $p = 0$ will dominate, while other monopoles will show strong higher order rotational symmetry due to the expansion coefficients other than zero being dominant. The eigenvector coefficients for each mode of a particular mode type, also determined along with the eigenvalues, facilitate the determination of the dominant features of modes and the localization with regards to the center of the pattern. The 69 available states calculated for the monopoles are plotted in Fig. 4 with the dominant expansion coefficient's rotational order along the ordinate axis versus wavelength. Modes with the strongest $p = 0$ expansion coefficients and relatively smaller higher order expansion coefficients will be dominated by a strong field confinement in the center of the structure and show little or no field variation with rotation angle. Examination of the eigenvector coefficient space reveals two strongly confined monopoles at wavelengths 1.00 μm and 1.55 μm. The radial extent of the dielectric structure was readjusted in order to provide a strong monopole at 1.55 μm thus the choice for a dielectric radius of $R = 3.91\ \mu m$. Since each mode in turn contains 7781 expansion coefficients, the mode's rotational symmetry properties are plotted versus rotational order, p, positive side only and by plotting the sum of the absolute value of the expansion coefficients in each rotational order. Fig. 5 shows the modal profile,H_z field distribution, and rotational properties for the two dominant monopoles. Both field profiles show a strong monopole located at the center of the dielectric which corresponds to the strong $p = 0$ expansion coefficients. The addition of the higher rotational symmetry orders introduces additional symmetries to the mode profile located in the ring region of the dielectric. Fig. 6 shows two other monopole type expansions, and the field distributions in which the central regions of the higher order rotational symmetries are equivalent to the lowest order monopole yet the field profiles contain strong 12-fold rotational orders.

In order to confirm the presence of the dominant modes determined using the Fourier-Bessel technique, the localized state spectrum and field profiles were also determined using the finite-difference time-domain technique (FDTD)[23, 24]. The dielectric structure was discretized to a 200 point per micron rectangular grid and bordered by a 400 grid point PML. A TE polarized point source was located at the center of the structure, contained wavelengths from 0.5 to 5.0 μm in 0.01 μm increments and run for the first 500 time iteration steps. The nature of the point source and its location excites only monopole states. The Fourier transform shown in Fig. 7 was obtained using the field values at the

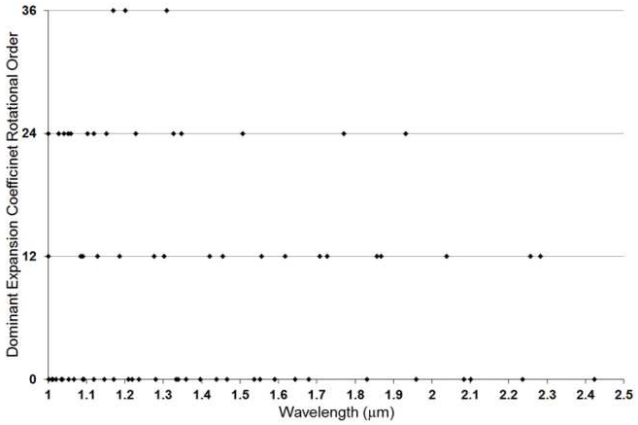

Figure 4. *State space returned for the dielectric structure shown in Fig. 1 (Center). Of the 7781 monopole solutions returned, 69 lie in the 1.0 to 2.5 μm wavelength range. Amongst these are those that display strong monopole properties as their expansion coefficients are dominated by the* $p = 0$ *rotational order. Monopoles displaying higher rotational symmetry are indicated by* $p = 12, 24, \ldots$

center for 150,000 computation time iteration steps and plotted for the 0.9 to 2.5 μm range. The trace confirms the presence of the two dominant monopole modes determined through the FB technique. In addition, the field profiles also shown in Fig. 7, computed using the FDTD technique, agree with the FB modes shown in Fig. 5. The field profiles shown in the insert were produced using the surface Fourier transform technique computed over 10,000 time iteration steps. The Fourier transform spectrum also indicates the presence of other modes of lesser amplitude of which two of these were identified as the FB modes in Fig. 6. In the FB results that follow, the states and spectrums were also confirmed using the FDTD technique. For the sake of keeping the presentation compact, the FDTD confirmations are not shown.

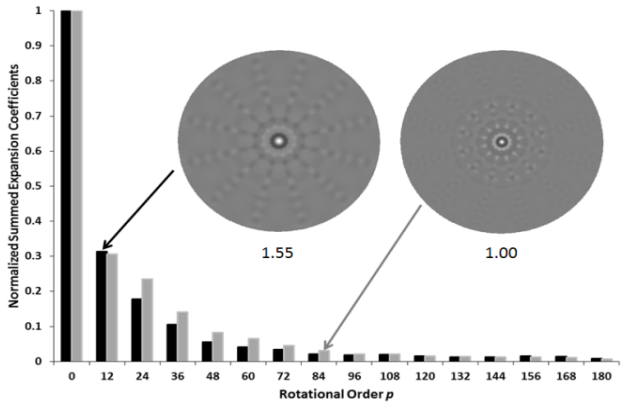

Figure 5. *Rotational order spectrum for selected modes showing strong* $p = 0$ *rotational order, (Right)* $\lambda = 1.00\ \mu m$ *and (Left)* $\lambda = 1.55\ \mu m$. *Insert is reconstructed modes from eigenvector coefficients and field expression (4). Magnitude of the field profiles plotted using a grey scale with white showing maximums and black showing minimum regions.*

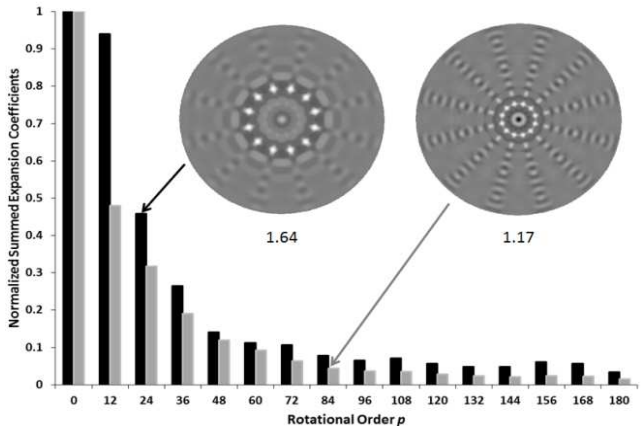

Figure 6. *Rotational order spectrum for selected modes showing strong $p = 0$ rotational order and significant higher order expansion coefficients, (Right) λ = 1.17 μm and (Left) λ = 1.64 μm. Insert is reconstructed mode from eigenvector coefficients and field expression (4). Magnitude of the field profiles plotted using a grey scale.*

When equation (6) is cast to solve for dipoles, the rotational order of the field expansion coefficients must be one of the following $(\pm 1, \pm 11, \pm 13, \pm 23, \pm 25, \ldots)$ which is obtained by setting $p' = \pm 1$ and m a symmetry order of the dielectric. As indicated above, the eigenmatrix for dipoles separates in two blocks, with one matrix returning the field expansion coefficient for the rotational orders $(+1, -11, +13, -23, +25, \ldots)$ and the other for the orders $(-1, +11, -13, +23, -25, \ldots)$. The full eigenvector for a particular eigenvalue is obtained by combining both sets of expansion coefficients. Fig. 8 shows the dipole state space returned for wavelengths in the 1.0 to 2.5 μm range. The dominant dipoles are determined by scanning through the eigenvector space and locating the strong coefficients at $p = 1$. Two of the dipole modes are shown in Fig. 9 for the wavelengths 1.27 and 1.99 μm. Two additional modes in the dipole grouping are shown in Fig. 10 where the higher order rotational symmetries dominate the modal profile.

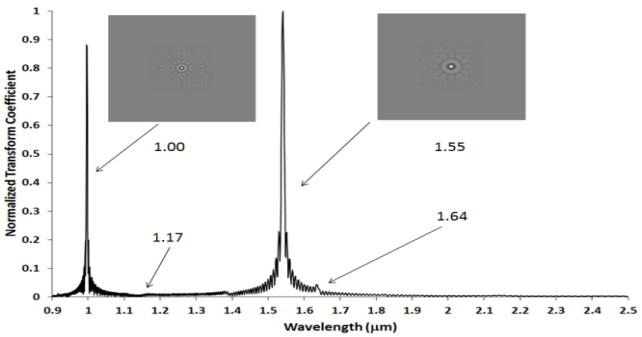

Figure 7. *Fourier spectrum space computed for the central transform point over the range of 0.9 to 2.5 μm. Dominant long lived modes correspond to the localized modes determined through examination of the eigenvector spectrum returned through FB analysis.*

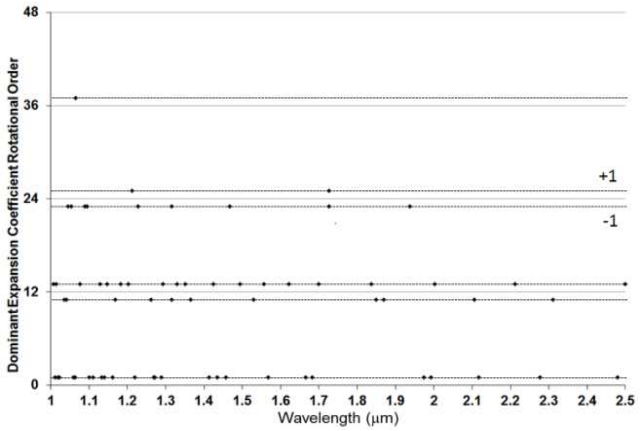

Figure 8. *Dipole state space determined through FB analysis for the 1.0 to 2.5 μm wavelength range. Dipoles are sorted based on dominant rotational order present in the eigenvector expansion coefficients. Dipole rotational space is split by ±1 compared to the rotational space of monopoles shown in Fig. 4.*

For the quadrupole states the eigenmatrix returns field expansion coefficients with rotationalorders $(\pm 2, \pm 10, \pm 14, \pm 22, \pm 26, \ldots)$. As with the dipoles, the eigenmatrix can be divided into two blocks that are individually solved. The eigenvectors of the states are produced by collecting all expansion coefficients for the same eigenvalue. Fig. 11 shows the state space for the quadrupoles obtained using the FB technique in the 1.0 to 2.5 μm range while Fig. 12 shows the rotational order space for two of the dominant modes present.

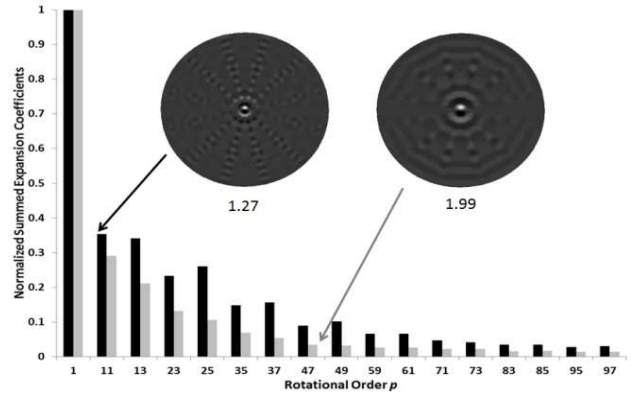

Figure 9. *Two of the dominant dipoles of the circular dielectric profile. The expansion coefficient space is dominated by the rotational order at $p = \pm 1$. The presence of the higher order symmetries produce field values in the rings where the higher order symmetries are present.*

5. Heterostructure

The analysis above indicates that the circular photonic crystal structure contains an array of available modes and

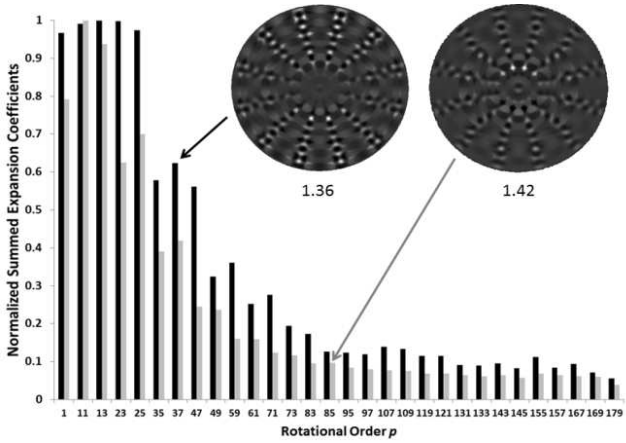

Figure 10. *Two representative dipole class modes which are dominated by expansion coefficients of order $p = \pm 11$ or higher. These modes extend strongly in the dielectric ring region demonstrating the strong interplay between dielectric and mode structure.*

those with strong monopole, dipole and quadrupole nature can be identified by examining the dominant expansion coefficients of the eigenvector. To further explore the state space properties, the 5 inner most rings of the circular dielectric are used to form the defect region for a translationally symmetric hexagonal array photonic crystal, Fig. 13. The hexagonal array is chosen to have circular air holes with radius $r = 0.271$ μm and lattice constant $a = 0.630$ μm in a silicon background, $r/a = 0.430$. The TE polarization band structure of the hexagonal array was calculated and a large band gap was identified between normalized frequencies of 0.273 and 0.461 corresponding to a wavelength range of 2.31 to 1.37 μm.

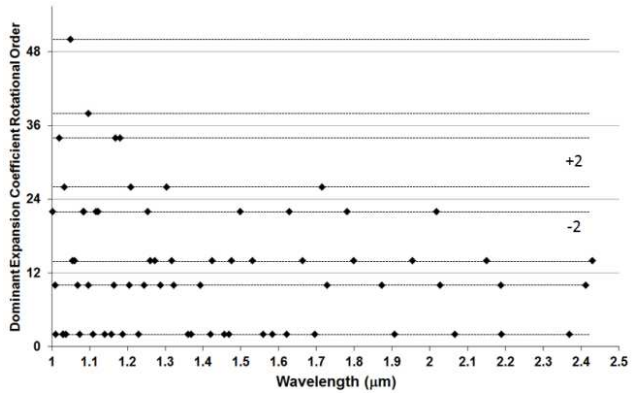

Figure 11. *State space for the quadrupole modes determined through the FB technique.Quadrupole rotational space is split by ±2 compared to the rotational space of monopoles shown in Fig. 4.*

The determination of the steady state space using the Fourier-Bessel technique analysis was performed on the heterostructure which has an overall 6-fold rotational symmetry that is imposed by the hexagonal lattice. The range R was set to 5 μm and was sufficient to contain the circular structure and a large portion of the hexagonal array. Fig. 14 shows the array of states determined when monopole type modal solutions are determined for the 1.0 to 2.5 μm wavelength range. These modes will have non-zero expansion coefficients of the associated eigenvector for rotational symmetries of $p = (0, \pm 6, \pm 12, \pm 18, \pm 24, \dots)$, imposed by the presence of the hexagonal array and are separated depending on the rotational order of the dominant expansion coefficient. On the lower wavelength side of the figure, below 1.37 μm, a large number of states are present and correspond to states that significantly extend into the hexagonal array and are not confined by the band gap. Above the upper band gap wavelength of 2.31 μm the low number of states returned is typical of the FB computation process as they correspond to long wavelength states that average the dielectric. Within the band gap several states that display the strongest lowest order $p = 0$ expansion coefficients are present. Three of the states are shown; the highly localized monopole at 1.55 μm, an interface state at 1.60 μm and a super state at 2.25 μm. Modes dominated by orders 6 and 12, not shown, display the same general features as those of order 0 but in general are less localized and can display features similar to whispering gallery modes.

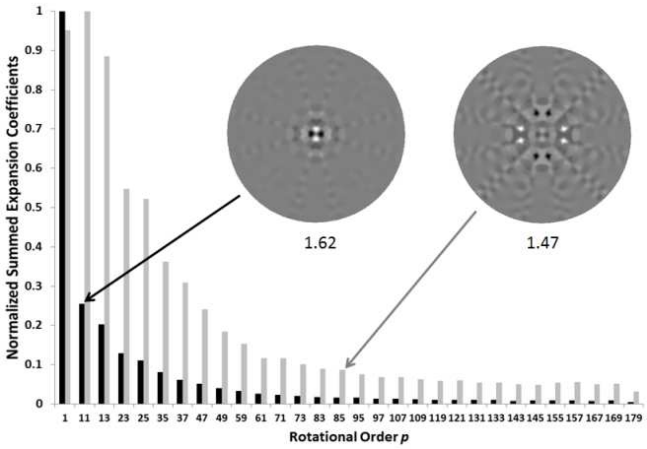

Figure 12. *Two representative quadrupole class modes. The left mode is dominated by the $p = \pm 2$ order and resembles a strongly localized state to the central disk of the dielectric profile. The right mode has strong rotational orders at $p = 2, 10, 12$ and shows that this mode extends into the ring region of the dielectric profile.*

Fig. 15 shows the expansion coefficients collected per angular order p for the three states indicated above. Since the monopole at 1.55 μm is primarily located within the circular dielectric region the expansion coefficient rotational order space is dominated by the 12-fold rotational symmetry and displays strong coefficients at multiples of ±12. Interlaced within the strong rotational orders and at multiples of 6 are the expansion coefficients due to the extension of the mode into the hexagonal array. The interface state mode at 1.60 μm displays a rotational order expansion space with strong dependence on the 6-fold hexagonal and 12-fold circular dielectric profiles. The slightly stronger coefficients in multiples of ±12 indicate that the mode is more highly present on the central circular structure. The super state mode at 2.25 μm has expansion

coefficients that extend, in deceasing amplitude, over the entire 6-fold space which includes the 12-fold rotational order. The presence of the inner circular structure is still observed as the height of rotational order 36 (multiple of 12) is higher than that of 30 (multiple of 6). The examination of the state space for the various modes returned by applying the FB technique to a heterostructure can return information on the type of mode the state represents.

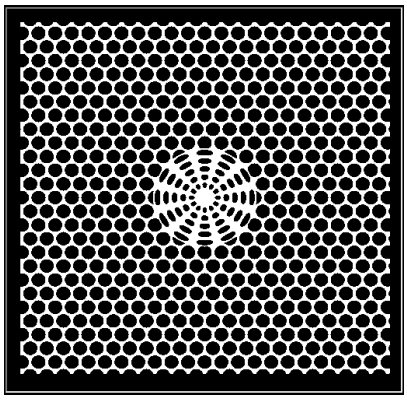

Figure 13. *Photonic crystal heterostructure composed of a translationally symmetric hexagonal array ($r/a = 0.430$) in which the central region had been replaced by the first 5 rings of the circular structure. White is silicon and black is air.*

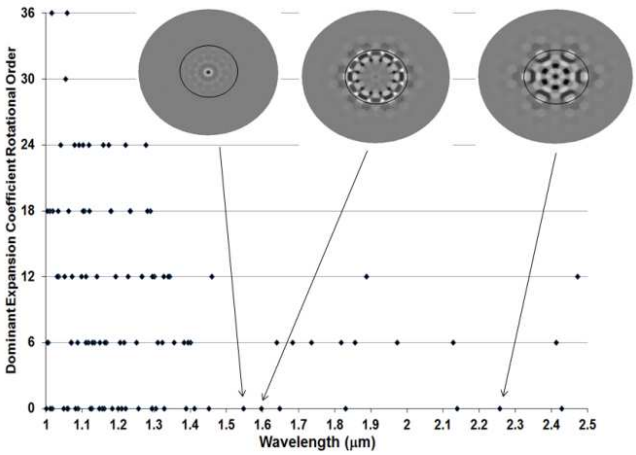

Figure 14. *State space for the monopole type solutions of the heterostructure shown in Fig. 13 (Left). The field profiles for three states, highly localized (1.55), interface (1.60) and super state (2.25) are shown which are present in the band gap region of the hexagonal array. The expansion coefficients of these states are shown in Fig. 15.*

Given that there are states confined to the inner circular dielectric and with wavelengths inside the band gap range of the hexagonal array, these modes are available as localized states and may be excited by coupling light from an adjacent waveguide. Two such waveguide configurations are shown in Fig. 16. The Fourier-Bessel technique can also be applied to explore the excitation of the modes by recognizing that the dielectric structures in Fig. 16 only have a rotational symmetry of 1. A total of 18100 expansion coefficients were used to compute the states of the structure $(n = 200, m = 90)$. Of the states available 2 for each waveguide configuration are shown in Fig. 17. The top left mode has a wavelength of 1.55 μm. Close examination shows that the mode also extends into the waveguide region and represents the field profile of the waveguide mode that will excite the strong monopole. The top right mode corresponds to the state at 1.60 μm. This mode has field extremes at the interface between the two dielectric structures corresponds to an interface state. The lower two states have the waveguide pushed one row of holes further away. In this way the presence of the waveguide, acting as a perturbation to the original heterostructure has less effect on central states that extend into the hexagonal region. The mode in lower left shows coupling to a strong dipole at 1.46 μm that extends over the entire inner region. The mode on the lower right is shown coupling to a mode at 1.54 μm showing strong 3-fold rotational symmetry. The field profiles in the waveguide region are the waveguide mode profiles at the corresponding wavelengths required to excite the mode.

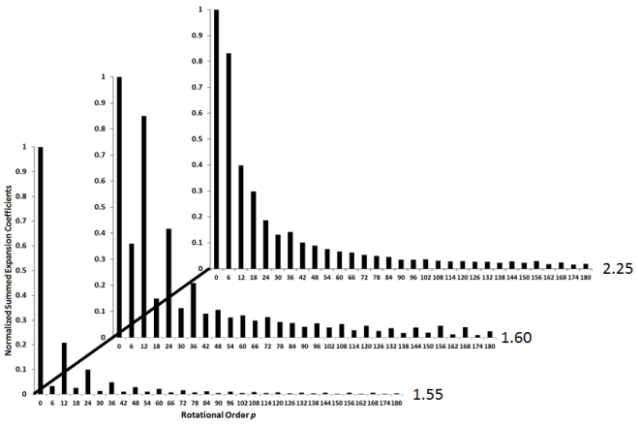

Figure 15. *Expansion coefficients collected by rotational order p for the highly localized monopole at 1.55 μm the interface state at 1.60 μm and the super state at 2.25 μm. The coefficient space for the first two states is dominated by the 12-fold symmetry of the inner circular dielectric. Midway between the dominant orders are the contributions from the symmetry of 6 imposed by the hexagonal array. The last state being a super state extends over the entire dielectric and as such shows strong 6 fold symmetry with a trace of the 12 fold remaining as order 36 is slightly higher than order 30.*

6. Conclusion

We have shown that a dielectric structure that contains both radial and angular periodicity supports a number of different centrally located states. The monopole, dipole and quadrupole states are determined by making use of a Fourier-Bessel equivalent of the plane-wave technique applied to the conventional Gamma point. The eigenmatrix can be tuned for a particular mode order and by examining the eigenvector coefficient space, the dominant states can be determined. We also show that the Fourier-Bessel technique can be used to analyze the states present in a heterostructure configuration and for configurations which make use of waveguides for exciting the localized states.

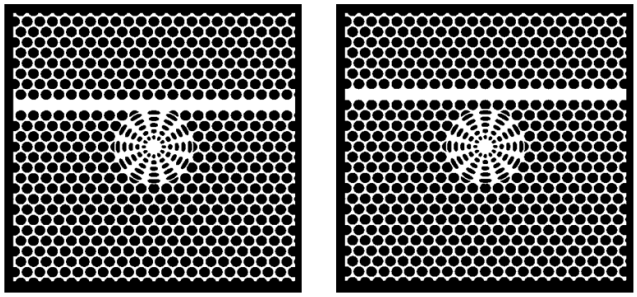

Figure 16. *Heterostructure waveguide configurations. The central circular dielectric has a radius of 1.96 μm and is composed of the 5 inner rings and central high dielectric region. (Left) waveguide located directly adjacent to the inner circular dielectric region. (Right) waveguide offset by one row of holes of the hexagonal array.*

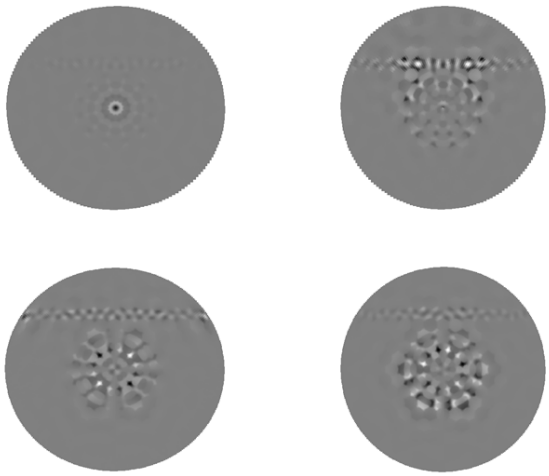

Figure 17. *The top mode profiles have waveguide adjacent to the inner circular dielectric region. (Top left) – mode at 1.55 μm, (Top right) – mode at 1.60 μm. Lower mode profiles have waveguide pushed one row of holes further away. (Bottom left) – mode at 1.46 μm, (Bottom right) – mode at 1.54 μm. In all cases the field profile in the waveguide region represents the waveguide field profile required to excite the particular mode.*

Acknowledgements

The authors acknowledge support from NSERC and Carleton University for this research effort.

References

[1] R. D. Meade, A. M. Rappe, K. D. Brommer and J. D. Joannopoulus, "Nature of the photonic band gap: some insights from a field analysis," J. Opt. Soc. Am. B. 10, 328-332 (1993).

[2] M. A. Kaliteevski, S. Brand, R. A. Abram, T. F. Krauss, R. Dela Rue and P. Millar, "Two-dimensional Penrose-tiles photonic quasicrystals: from diffraction pattern to band structure," Nanotechnology 11, 274-280 (2000).

[3] A. Massaro, R. Cingolani, M. Vittorio and A. Passaseo, "Artificial anisotropy in circular photonic crystals andapplications," IEEE Transc. On Nanotech. 9, 157-169 (2010).

[4] W. Zhong and X. Zhang, "Localized modes in defect-free two-dimensional circular photonic crystal," Phys. Rev. A81, 013805 (2010).

[5] N. Horiuchi, Y. Segawa, T. Nozokido, K. Mizuno and H. Miyazaki, "Isotropic photonic gaps in circular photonic crystal," Opt. Let. 29, 1084-1086 (2003).

[6] A. Massaro, V. Tasco, M. Todaro, T. Stomeo, R. Cingolani, M. Vittorio and A. Passaseo, "FEM design and modeling of $\chi^{(2)}$ second-harmonig enhancement in circular photonic crystal," J. Lightwave Technol. 27, 4262-4268 (2009).

[7] J. Omero-Vivas, D. N. Chirgrin, A. V. Lavrinenko and C. M. Sotomayor Torres, "Resonant add-drop filter based on a photonic quasicrystal," Opt. Exp. 13, 826-835 (2005).

[8] P. Lee, T. Lu, M. Yu and C. Tseng, "Photonic crystal circular-shaped microcavity and its uniform cavity-waveguide coupling property due to presence of whispering gallery mode," Opt. Exp. 15, 9450-9457 (2007).

[9] P. Lee, T. Lu, J. Fan and F. Tsai, "High quality factor microcavity lasers realized by circular photonic crystal with isotropic photonic band gap effect," Appl. Phys. Let. 90, 151125 (2007).

[10] J. Zarbakhsh, A. Mohtashami and K. Hingerl, "Geometrical freedom for constructing variable size photonic bandgap structures," Opt. and Quant. Electron., 39, 395-405, (2007).

[11] J. Chaloupka, J. Zarbakhsh and K. Hingerl, "Local density of states and modes of circular photonic crystal cavities," Phys. Rev. B 72, 085122 (2005).

[12] P. Lee, T. Wu., F. Tsai and T. Lu, "Investigation of whispering gallery mode dependence on cavity geometry of quasiperiodic photonic crystal microcavity lasers," Appl. Phys. Let. 89, 231111 (2006).

[13] K. Ueda, T. Dotera, and T. Gemma, "Photonic band structure calculations of two-dimensional Archimedean tiling patterns," Phys. Rev. B. 75 195122 (2007).

[14] W. Steurer and D. Sutter-Widmer, "Photonic and phononicquasicrystals," J. Phys. D 40, R229-R247 (2007).

[15] M Rechtsman, H. Jeong, P. Chaikin, S. Torquato and P. Steinhardt, "Optimized structures for photonic quasicrystals," Phys. Rev. Lett. 101, 073902, (2008).

[16] R. Gauthier, "Perfect periodic photonic quasi-crystals," Proc. SPIE 6901, 69011F (2008).

[17] D. Chang, J. Scheuer and A. Yariv, "Optimization of circular photonic crystal cavities – beyond coupled mode theory," Opt. Exp. 13, 9272-9279 (2005).

[18] J. Scheuer and A. Yariv, "Coupled-waves approach to the design and analysis of Bragg and photonic crystal annular resonators," IEEE J. Quant. Electron. 39, 1555-1562 (2003).

[19] J. Scheuer and A. Yariv, "Circular photonic crystal resonator," Phys. Rev. E 70 036603 (2004).

[20] S. R. Newman and R. C. Gauthier, "Representation of photonic crystals and their localized modes through the use of Fourier-Bessel expansions," J. IEEE Photon. 3, 1133-1141 (2011).

[21] J. D. Joannopoulos, R.C. Meade, J. N. Winn, *Photonic crystals: molding the flow of light* (Princeton University

Press, 1995).

[22] S. R. Newman and R. C. Gauthier, "Fourier-Bessel analysis of localized states and photonic bandgaps in 12-fold photonic quasi-crystals," J. Opt. Soc. Am. A 29, 2344-2349 (2012).

[23] R. Gauthier, K. Mnaymneh, S. Newman, K. Medri and C. Raum, "Hexagonal array photonic crystal with photonic quasi-crystal defect inclusion," Opt. Materials 31, 51-57 (2008).

[24] S. Newman and R. Gauthier, "FDTD sources for localized state excitation in photonic crystals and photonic quasi-crystals," Proc. SPIE 7223, 7940G (2009).